International Journal of Solids and Structures 49 (2012) 2881–2885

Contents lists available at SciVerse ScienceDirect

International Journal of Solids and Structures

journal homepage: www.elsevier.com/locate/ijsolstr

Mechanically tunable phononic band gaps in three-dimensional periodic elastomeric structures

Lifeng Wang [a], Katia Bertoldi [b,*]

[a] Department of Civil and Environmental Engineering, Clarkson University, Postdam, NY 13699, USA
[b] School of Engineering and Applied Sciences, Harvard University, Cambridge, MA 02139, USA

ARTICLE INFO

Article history:
Available online 31 May 2012

Keywords:
Phononic
Elasticity
Large deformations

ABSTRACT

Three-dimensional periodic structures have many applications in acoustics and their properties are strongly related to structural details. Here we demonstrate through simulations the ability to tune the phononic band gaps of 3D periodic elastomeric structures using deformation. The elastomeric nature of the material makes the transformation of the band gaps a reversible and repeatable process, providing avenues for the design of tunable 3D phononic crystals such as sonic switches.

1. Introduction

Three-dimensional periodic structures are of great interest because of their unique capability to interact with waves. Phononic crystals are periodic elastic structures designed to control the propagation of mechanical waves (Sigalas and Economou, 1992; Kushwaha et al., 1993; Sigalas et al., 2005; Maldovan and Thomas, 2006) and have exciting applications such as sound filters, acoustic wave guides and acoustic mirrors (Maldovan and Thomas, 2009; Qi et al., 2004; Cheng et al., 2006; Jang et al., 2009, 2007). The most fundamental property of phononic crystals is the existence of band gaps—a range in frequency where elastic waves propagation is barred. Thus incoming mechanical waves with frequencies within the band gap are totally reflected by the phononic crystal. Moreover, when a wave with frequency within a complete band gap is generated inside the structure, it is trapped near its source since its propagation is barred.

Phononic band gaps (PBGs) are caused by changes of the speed of sound in the crystal, so that their position and width strongly depend on the contrast in density and speed of sound of the constituent materials, the volume fraction of inclusions (Sainidou et al., 2002), lattice spacing and topology (Gorishnyy et al., 2005). The tunability of PBG is also of great interest, leading to the design of novel acoustic switches with properties that change upon the activation of an external stimulus. Interestingly, a recent study demonstrated that large deformation may be used to tune and transform the phononic band gaps of 2D soft periodic solids (Bertoldi and Boyce, 2008a,b).

3D Polydimethylsiloxane (PDMS) structures with complex architecture have been successfully fabricated using interference lithography (Jang et al., 2006b; Yang et al., 2002; Campbell et al., 2000). Moreover, Brillouin light scattering measurements have shown that a moderate (30%) tensile in-plane deformation alters the phononic band gaps due to the change of sample lattice parameter and symmetry (Jang et al., 2006a). In this paper we explore through simulations the effect of large deformation of 3D periodic elastomeric structures on their phononic band gaps.

2. Modeling

Here we focus on the same 3D periodic elastomeric structure experimentally investigated by Jang et al. (Jang et al., 2006a,b; Wang et al., 2009). The volume fraction of solid is $\sim 26\%$ and the microstructure has three-fold symmetry along the two-axis, as shown in Fig. 1. Both the non-linear response of the structure and the dispersion diagram are investigated using the non-linear finite element code ABAQUS. Therefore, after characterization of the material (Section 2.1) analysis of the behavior of the infinite periodic arrays involves the following three steps:

- identification of a spatially periodic representative volume element (RVE) (Section 2.2);
- definition of appropriate boundary conditions (Section 2.3);
- waves propagation analysis accounting for pre-stress (Section 2.4).

2.1. Governing equations and material behavior

The stress–strain behavior of the PDMS elastomeric matrix is captured using a nearly incompressible nonlinear Neo–Hookean hyperelastic model, thus enabling large deformation and distortion in the 3D periodic structure (Ogden, 1984).

* Corresponding author.
E-mail address: bertoldi@seas.harvard.edu (K. Bertoldi).

0020-7683/$ - see front matter © 2012 Elsevier Ltd. All rights reserved.
http://dx.doi.org/10.1016/j.ijsolstr.2012.05.008

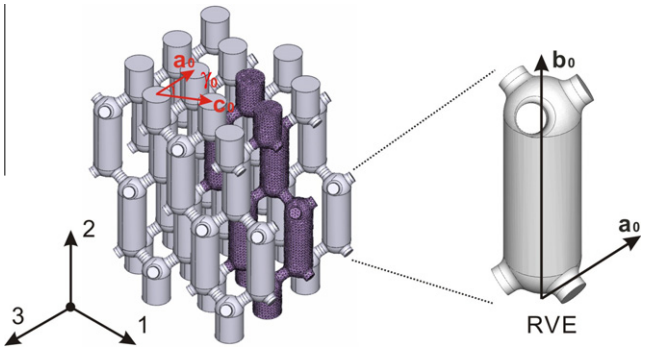

Fig. 1. Schematic of the considered 3D periodic structure and RVE. $\mathbf{a}_0 = [0 \quad 0 \quad 975]$ nm, $\mathbf{b}_0 = [0 \quad 1425 \quad 0]$ nm and $\mathbf{c}_0 = [975\sin\gamma_0 \quad 0 \quad 975\cos\gamma_0]$ nm are the three independent lattice vectors in the undeformed configuration, with $\gamma_0 = 60^\circ$.

Let us consider a deformation described by the function $\boldsymbol{\chi}$ that maps a point $\mathbf{x}_0$ in the reference configuration to its deformed position $\mathbf{x} = \boldsymbol{\chi}(\mathbf{x}_0, t)$ in the current configuration. The associated deformation gradient will be denoted by $\mathbf{F} = \partial\mathbf{x}/\partial\mathbf{x}_0$, while J identifies its determinant, $J = \det\mathbf{F}$.

Using $\mathbf{x}_0$ and t as independent variables, the equations of motion in absence of body forces are given by (Ogden, 1984)

$$\mathrm{Div}\mathbf{S} = \rho_0 \frac{D^2\boldsymbol{\chi}}{Dt^2}, \tag{1}$$

where $\mathbf{S}$ denotes the first Piola–Kirchoff stress tensor, ρ_0 the density in the reference configuration, D/Dt the material time derivative and Div the divergence operator in the reference configuration. If the body is at rest $D^2\boldsymbol{\chi}/Dt^2$ vanishes everywhere, so that Eq. (1) reduces to the static equilibrium equation

$$\mathrm{Div}\mathbf{S} = \mathbf{0}. \tag{2}$$

Here, we focus on an isotropic hyperelastic material whose strain energy density W can be expressed as a function of the invariants of the right Cauchy–Green tensor $\mathbf{C} = \mathbf{F}^T\mathbf{F}$ (or, alternatively, also the left Cauchy–Green tensor $\mathbf{B} = \mathbf{F}\mathbf{F}^T$),

$$W = W(I_1, I_2, I_3), \tag{3}$$

where

$$I_1 = \mathrm{tr}\mathbf{C}, \quad I_2 = \frac{1}{2}\left[(\mathrm{tr}\mathbf{C})^2 - \mathrm{tr}\mathbf{C}^2\right], \quad I_3 = \det\mathbf{C} = J^2, \tag{4}$$

I_1 being essentially a scalar equivalent stretch measure and I_3 the square of the volume ratio. The stress–strain behavior of PDMS is modeled using a Neo–Hookean model (Ogden, 1984) (modified to include compressibility with a high bulk modulus):

$$W(I_1, I_3) = \frac{\mu}{2}(I_1 - 3) + \mu\log J + \frac{K}{2}(J-1)^2, \tag{5}$$

where μ is the initial shear modulus and K is the bulk modulus. The Cauchy stress, is given by

$$\boldsymbol{\sigma} = \frac{2}{J}\frac{\partial W}{\partial I_1}\mathbf{B} + \frac{\partial W}{\partial J}\mathbf{I}, \tag{6}$$

yielding

$$\boldsymbol{\sigma} = \frac{\mu}{J}\mathbf{B} + \left[K(J-1) - \frac{\mu}{J}\right]\mathbf{I}, \tag{7}$$

with corresponding first Piola–Kirchoff stress $\mathbf{S}$ found as

$$\mathbf{S} = J\boldsymbol{\sigma}\mathbf{F}^{-T} = \mu\mathbf{F} + J\left[K(J-1) - \frac{\mu}{J}\right]\mathbf{F}^{-T}. \tag{8}$$

In this study we used $\mu = 0.8$ MPa and $K = 1$ GPa, while the elastomer density is 1050 kg/m^3.

2.2. Identification of a spatially periodic representative volume element

The non-linear response of the periodic structure is investigated using 3D micromechanical modeling (Wang et al., 2009; Jang et al., 2006b). This technique uses the constituent material stress–strain behavior together with a periodic representative volume element (RVE) of the microstructure and captures the infinite periodic nature of the structure through periodic boundary conditions (Section 2.3). Any arbitrary macroscopic deformation gradient can be applied to the RVE and the analysis captures details of the underlying deformation mechanisms. For the considered structure the RVE comprises of a thicker vertical post (with a diameter of 500 nm and a length of 1100 nm) and six thinner obliquely oriented struts (with a diameter of 200 nm and a length of 320 nm) (see Fig. 1). The periodicity of the undeformed structure is 975 nm in the transverse plane (1–3 plane) and 1425 nm in the normal direction (2-direction) and it is fully characterized by the three lattice vectors $\mathbf{a}_0 = [0 \quad 0 \quad 975]$ nm, $\mathbf{b}_0 = [0 \quad 1425 \quad 0]$ nm and $\mathbf{c}_0 = [975\sin\gamma_0 \quad 0 \quad 975\cos\gamma_0]$ nm with the initial in-plane interaxial angle $\gamma_0 = 60^\circ$, as shown in Fig. 1. The RVE is discretized using 10-node hybrid tetrahedron elements (C3D10H in ABAQUS/Standard element library, Providence, RI).

2.3. Boundary conditions

To subject an RVE to a macroscopic deformation gradient periodic boundary conditions are imposed on all cell boundaries such that

$$\mathbf{u}_B - \mathbf{u}_A = (\overline{\mathbf{F}} - \mathbf{I})[\mathbf{x}_{0B} - \mathbf{x}_{0A}] = \overline{\mathbf{H}}[\mathbf{x}_{0B} - \mathbf{x}_{0A}], \tag{9}$$

where A and B are two points periodically located on the RVE boundary. In Eq. (9), $\overline{\mathbf{H}} = 1/\Omega\int_\Omega \mathbf{H}dV = \overline{\mathbf{F}} - \mathbf{I}$ denotes the macroscopically applied displacement gradient and $\mathbf{u} = \mathbf{x}(\mathbf{x}_0) - \mathbf{x}_0$ denotes the displacement at $\mathbf{x}_0$. The macroscopic deformation is imposed by prescribing the nine components of $\overline{\mathbf{H}}$, which are viewed as generalized degrees of freedom operationally applied using a set of virtual nodes. The macroscopic first Piola–Kirchoff stress tensor and the corresponding macroscopic Cauchy stress tensor are then extracted through virtual work considerations (Danielsson et al., 2002). Rigid body motion is prevented by constraining the displacements of a single point. In this study each RVE is subjected to macroscopic uniaxial tension applied along directions 1 and 2; uniaxial tension applied along direction 1 yields

$$\overline{\mathbf{H}} = (\lambda - \mathbf{1})\hat{\mathbf{e}}_\mathbf{1} \otimes \hat{\mathbf{e}}_\mathbf{1} + \overline{\mathbf{H}}_{\mathbf{22}}\hat{\mathbf{e}}_\mathbf{2} \otimes \hat{\mathbf{e}}_\mathbf{2} + \overline{\mathbf{H}}_{\mathbf{33}}\hat{\mathbf{e}}_\mathbf{3} \otimes \hat{\mathbf{e}}_\mathbf{3}, \tag{10}$$

where by $\overline{H}_{11} = \lambda - 1$ is imposed (λ is referred to as "load parameter") and $\overline{H}_{22}$ and $\overline{H}_{33}$ are not prescribed and determined by the condition $\overline{S}_{22} = \overline{S}_{33} = 0$. Similarly for uniaxial tension applied along direction 2 $\overline{\mathbf{H}}$ is given by

$$\overline{\mathbf{H}} = \overline{\mathbf{H}}_{\mathbf{11}}\hat{\mathbf{e}}_\mathbf{1} \otimes \hat{\mathbf{e}}_\mathbf{1} + (\lambda - \mathbf{1})\hat{\mathbf{e}}_\mathbf{2} \otimes \hat{\mathbf{e}}_\mathbf{2} + \overline{\mathbf{H}}_{\mathbf{33}}\hat{\mathbf{e}}_\mathbf{3} \otimes \hat{\mathbf{e}}_\mathbf{3}, \tag{11}$$

where $\overline{H}_{11}$ and $\overline{H}_{33}$ are not prescribed and determined by the condition $\overline{S}_{11} = \overline{S}_{33} = 0$.

2.4. Waves propagation

Let us consider a perturbation superimposed upon a given state of finite deformation that takes the body to a new equilibrium configuration where Eq. (1) are still satisfied. This incremental problem is governed by

$$\mathrm{Div}\dot{\mathbf{S}} = \rho_0 \frac{D^2\dot{\mathbf{x}}}{Dt^2}. \tag{12}$$

Assuming that all incremental quantities are sufficiently small, the constitutive Eq. (8) can be linearized as

$$\dot{\mathbf{S}} = \mathbb{L}\dot{\mathbf{F}}, \quad \text{with} \quad \mathbb{L}_{ijkl} = \frac{\partial^2 W}{\partial F_{ij}\partial F_{kl}}, \tag{13}$$

where $\dot{\mathbf{F}} = \partial\dot{\mathbf{x}}/\partial\mathbf{x}_0$. For an incremental wave motion characterized by a frequency of vibration ω

$$\dot{\mathbf{x}}(\mathbf{x}_0, t) = \dot{\boldsymbol{\kappa}}(\mathbf{x}_0)\exp[-\mathrm{i}\omega t], \tag{14}$$

the stress is also complex valued

$$\dot{\mathbf{S}} = \dot{\boldsymbol{\mathcal{S}}}\exp[-\mathrm{i}\omega t]. \tag{15}$$

Substitution of Eqs. (14) and (15) into Eq. (12) yields

$$\mathrm{Div}\dot{\boldsymbol{\mathcal{S}}} + \rho_0\omega^2\dot{\boldsymbol{\kappa}} = \mathbf{0}. \tag{16}$$

To investigate the effect of deformation on the PBGs, the propagation of elastic waves through the 3D structure is analyzed at different levels of macroscopic strain. The band structure is calculated conducting a Bloch-wave analysis within the finite-element framework (Bertoldi and Boyce, 2008a; Bertoldi and Boyce, 2008b). In order to work with the complex-valued displacements of the Bloch-wave calculation within the confines of ABAQUS, all fields ψ are split into real and imaginary parts

$$\psi(\mathbf{x}_0) = \psi^{Re}(\mathbf{x}_0) + \mathrm{i}\psi^{Im}(\mathbf{x}_0). \tag{17}$$

In this way the incremental equations of motion (16) split into two sets of uncoupled equations for the real and imaginary parts,

$$\begin{aligned} &\mathrm{Div}\dot{\boldsymbol{\mathcal{S}}}^{Re} + \rho_0\omega^2\dot{\boldsymbol{\kappa}}^{Re} = 0, \\ &\mathrm{Div}\dot{\boldsymbol{\mathcal{S}}}^{Im} + \rho_0\omega^2\dot{\boldsymbol{\kappa}}^{Im} = 0. \end{aligned} \tag{18}$$

Then the problem is solved using two identical finite-element meshes for the RVE – one for the real part and one for the imaginary part – and coupling them by Bloch-type displacement boundary conditions (Kittel, 1986)

$$\begin{aligned} \dot{\boldsymbol{\kappa}}^{Re}(\mathbf{x}_0 + \mathbf{r}_0) &= \dot{\boldsymbol{\kappa}}^{Re}(\mathbf{x}_0)\cos[\mathbf{K}_0\cdot\mathbf{r}_0] - \dot{\boldsymbol{\kappa}}^{Im}(\mathbf{x}_0)\sin[\mathbf{K}_0\cdot\mathbf{r}_0], \\ \dot{\boldsymbol{\kappa}}^{Im}(\mathbf{x}_0 + \mathbf{r}_0) &= \dot{\boldsymbol{\kappa}}^{Re}(\mathbf{x}_0)\sin[\mathbf{K}_0\cdot\mathbf{r}_0] + \dot{\boldsymbol{\kappa}}^{Im}(\mathbf{x}_0)\cos[\mathbf{K}_0\cdot\mathbf{r}_0], \end{aligned} \tag{19}$$

$\mathbf{r}_0$ being a vector that defines the distance in the reference configuration between two periodically located nodes. After finite element discretization of Eq. (18) and application of the incremental boundary displacements (19) the eigenfrequencies ω can be computed for any wave vector $\mathbf{K}_0$ and for any level of finite deformation defined by $\bar{\mathbf{F}}$ (Bertoldi and Boyce, 2008a,b).

3. Results

3.1. Non-linear response

In this study macroscopic uniaxial tension applied along direction 1 and 2 is considered. Results for the macroscopic nominal stress vs nominal strain ($\epsilon = \lambda - 1$) behavior up to a tensile strain of 1.0 are shown in Fig. 2a. The initial Young's modulus of the structure is 46 kPa and 265 kPa for tensile loading in direction 1 and 2, respectively. Local features of deformation are shown in the contours of von Mises stress at different level of deformation reported in Fig. 2b. The snapshots clearly show that the deformation is mostly accommodated by the diagonal struts. When uniaxial tension is applied along direction 1, the diagonal struts simultaneously stretch and rotate. In the case of uniaxial tension in direction 2 all struts are highly stretched and transfer the load to the vertical post, providing higher stiffness. Interestingly elasto-plastic structures characterized by the same architecture show a different deformation mechanism, where deformation spreads to the thick posts after yielding (Wang et al., 2009).

It is clear from the snapshots (Fig. 2b) that the deformation largely changes both the sample lattice parameter and the symmetry

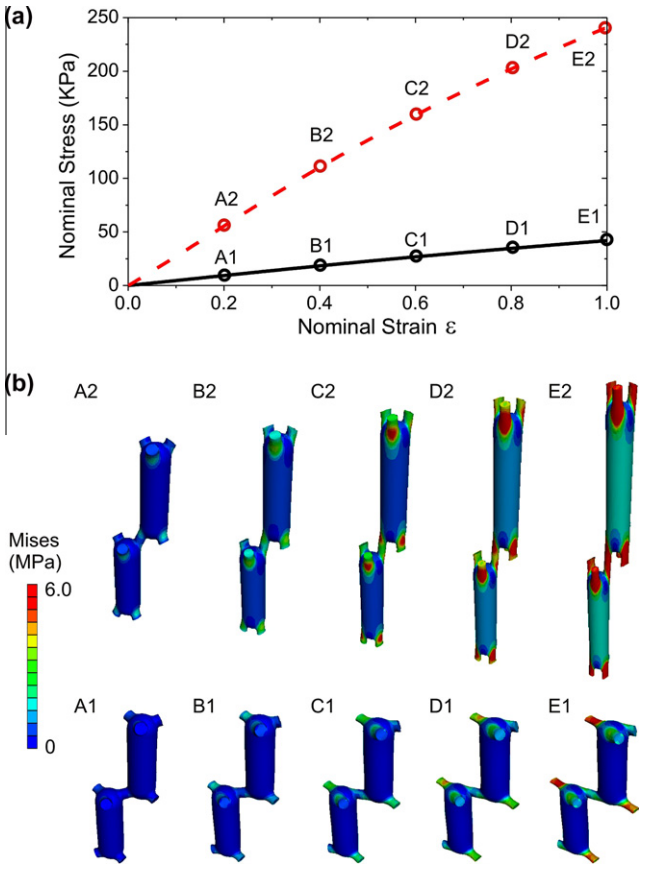

Fig. 2. Mechanical response of the considered 3D periodic structure under uniaxial tension. (a) stress–strain curves under tension along direction 1 (solid line) and 2 (dashed line). (b) Snapshots of the corresponding simulated deformed structures and von Mises stress contours at macroscopic strains of 0.2, 0.4, 0.6, 0.8, and 1.0.

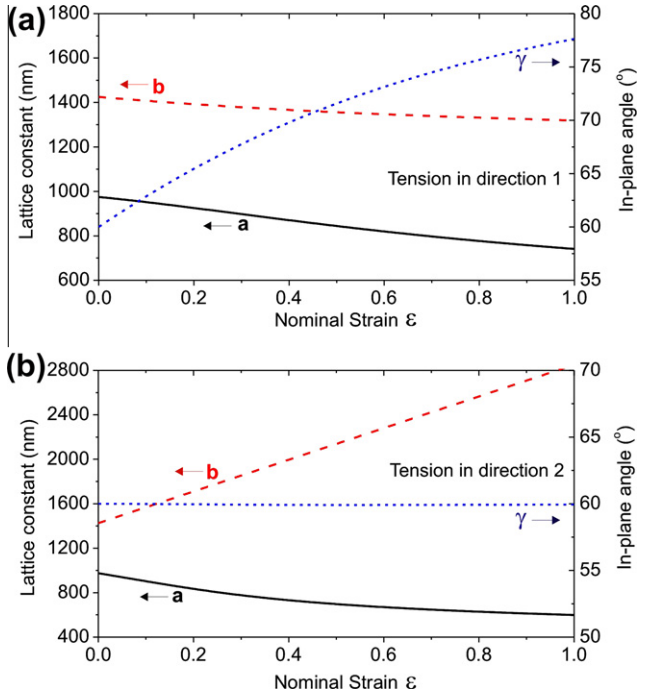

Fig. 3. (a) Lattice constants evolution as a function of strain for uniaxial tension along direction 1 (both periodicity and symmetry of the lattice change). (b) Lattice constants evolution as a function of strain for uniaxial tension along direction 2 (lattice periodicity changes).

of the periodic structure, thus providing a mechanism to alter the PBGs of the structure. Fig. 3(a) and (b) report the evolution of the magnitude of the two lattice vectors **a** and **b** and the in-plane inter-axial angle γ as a function of the applied deformation. When the structure is stretched, the lattice vector along the loading direction elongates and the lattice vector in the transverse direction contracts, thus changing the periodicity of the structure. Furthermore, when the structure is stretched along direction 1 (in the 1–3 plane), the increase of the in-plane angle γ indicates the breaking of the structural in-plane symmetry. Differently, when the structure is stretched along direction 2, the in-plane angle remain constant and the in-plane symmetry is preserved.

3.2. Waves propagation

We start by investigating the complete three-dimensional PGBs of the phononic crystal surrounded by vacuum. Hence we look for ranges in frequency where the propagation of both longitudinal and transverse elastic waves through the structure is not allowed irrespectively of their propagation direction in three dimensions. The evolution of the complete three-dimensional PGBs as a function of the applied deformation is reported in Fig. 4(a) and (b) for uniaxial tension applied along direction 1 and 2, respectively. In the undeformed configuration the periodic structure possesses a complete band gap for $\tilde{\omega} = \omega a_0/(2\pi c_{t0}) = 1.25 - 1.28$, where $a_0 = 975$ nm is the lattice constant in the 1–3 plane for the undeformed structure and $c_{t0} = 27.6$ m/s is the transverse speed of sound in the undeformed elastomeric material ($c_{l0} = 976.7$ m/s is the longitudinal speed of sound). Therefore elastic waves with frequency $f = \omega/(2\pi)$ in the range, $3.53 - 3.62 \cdot 10^7$ Hz are not allowed to propagate within the undeformed 3D structure. For both loading cases the complete band gap is observed to reduce progressively its width with deformation up to closure occurring at $\epsilon = 0.5$ and 0.9 for uniaxial tension in direction 1 and direction 2, respectively.

The evolution of PGBs for waves with propagation limited to the 1–3 plane perpendicular to the thick post ($\mathbf{K}_0 = [K_{01} \quad 0 \quad K_{03}]$) is presented in Fig. 4(c) and (d). In this case the undeformed structure is characterized by two separate in-plane PBGs for $\tilde{\omega} = [1.13 - 1.15, 1.23 - 1.29]$. For uniaxial tension along direction 1 (see Fig. 4(c)) only the second band gap is observed to close at $\epsilon = 0.9$, while the fist band gap is marginally affected by deformation. Moreover a new band gap $\tilde{\omega} = 0.39 - 0.41$ is formed when $0.3 < \epsilon < 0.9$. For uniaxial tension along direction 2 (see Fig. 4(d)) both the PGBs existing in the undeformed configuration are observed to close at $\epsilon = 0.9$, while during loading three new PBGs centered at $\tilde{\omega} = [0.33, 0.72, 0.80]$ open at $\epsilon = 0.3, 0.5$, and 0.7, respectively. These results are consistent with Brillouin light scattering measurements that have shown a shift in the band diagram for 30% applied in-plane tensile strain (Jang et al., 2006a). Finally we note that all the gaps observed in the structure investigated here are Bragg gaps (Jang et al., 2006a).

4. Conclusions

In conclusion, the Finite Element Method has been used to calculate the band structure of periodic three-dimensional structures at different levels of deformation and the proposed approach fully accounts for the effect of nonlinear deformation on the propagation of elastic waves. The method is extremely flexible and can be applied to the analysis of 3D periodic structures of arbitrary geometry and constituent material and subjected to any loading condition. The numerical analyses show that large deformation has a strong effect on the band structure of 3D periodic elastomeric structures and indicate the exciting possibility of using non-linear deformation to tune reversibly the PBGs of elastomeric phononic crystals.

Here, motivated by a recent experimental study (Jang et al., 2006a), we considered a structure characterized by ~26% volume fraction of solid and investigate the evolution of the band-gaps

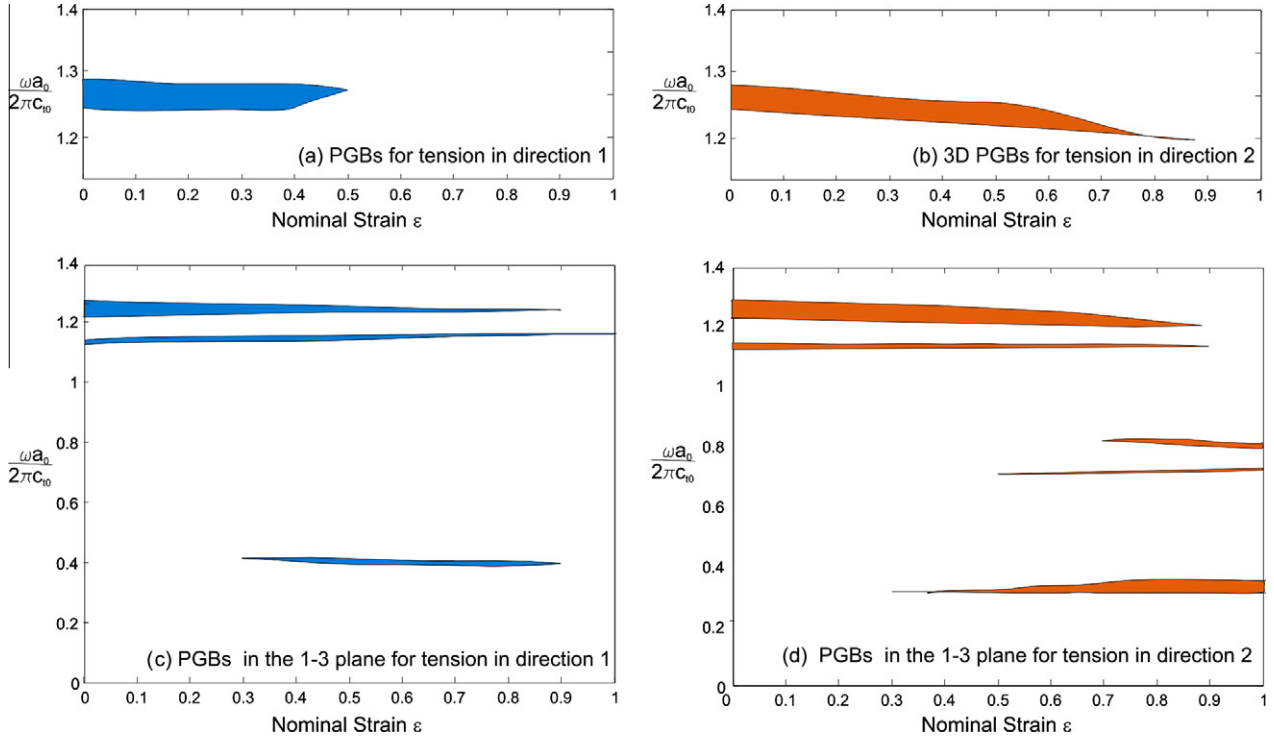

Fig. 4. Non-dimensional PGBs frequencies $\omega a_0/(2\pi c_{t0})$ for the considered 3D periodic structure as a function of the applied strain. (a,b): Complete three-dimensional PBGs versus nominal strain for loading along direction 1 (a) and direction 2 (b). (c,d): PGBs for waves propagating in the 1–3 plane versus nominal strain for loading along direction 1 (c) and direction 2 (d).

as a function of the applied deformation. Obviously a different choice of filling fraction would lead to PBGs with different location and width in the undeformed configuration. However, also in this case we would be able to use deformation to tune their width and location.

Finally, although in this study the stress–strain behavior of the elastomeric matrix is captured using a nearly incompressible Neo–Hookean hyperelastic model, the effect of stiffening in the material response on the PBGs could be easily included in the analysis. The stiffening effect is expected to strongly influence the band gaps of the periodic structure with deformation, since the privileged directions induced inside the elastomeric material by the deformation play an important role (Bertoldi and Boyce, 2008b).

Acknowledgements

L.F.W. gratefully acknowledges the financial support of the U.S. Army through the Institute for Soldier Nanotechnologies (ISN), under contract W911NF-07-D-0004. K.B. acknowledges Kavli Institute at Harvard University for financial support. L.F.W. and K.B. thank Professor Mary C. Boyce for useful discussions.

References

Bertoldi, K., Boyce, M.C., 2008a. Mechanically-triggered transformations of phononic band gaps in periodic elastomeric structures. Phys. Rev. B 77, 052105.
Bertoldi, K., Boyce, M.C., 2008b. Wave propagation and instabilities in monolithic and periodically structured elastomeric materials undergoing large deformations. Phys. Rev. B 78, 184107.
Campbell, M., Sharp, D.N., Harrison, M.T., Denning, R.G., Turberfield, A.J., 2000. Fabrication of photonic crystals for the visible spectrum by holographic lithography. Nature 404, 53–56.
Cheng, W., Wang, J.J., Jonas, U., Fytas, G., Stefanou, N., 2006. Observation and tuning of hypersonic bandgaps in colloidal crystals. Nat. Mater. 5, 830–836.
Danielsson, M., Parks, D.M., Boyce, M.C., 2002. Three-dimensional micromechanical modeling of voided polymeric materials. J. Mech. Phys. Solids 50, 351–379.
Gorishnyy, T., Ullal, C.K., Maldovan, M., Fytas, G., Thomas, E.L., 2005. Hypersonic phononic crystals. Phys. Rev. Lett. 94, 115501.
Jang, J.-H., Ullal, C.K., Gorishnyy, T., Tsukruk, V.V., Thomas, E.L., 2006a. Mechanically tunable three-dimensional elastomeric network/air structures via interference lithography. Nano Lett. 6, 740–743.
Jang, J.-H., Ullal, C.K., Choi, T., Lemieux, M.C., Tsukruk, V.V., Thomas, E.L., 2006b. 3D polymer microframes that exploit length-scale-dependent mechanical behavior. Adv. Mater. 18, 2123–2127.
Jang, J.-H., Ullal, C.K., Maldovan, M., Gorishnyy, T., Kooi, S., Koh, C.Y., Thomas, E.L., 2007. 3D micro- and nanostructures via interference lithography. Adv. Func. Mater. 17, 3027–3041.
Jang, J.-H., Koh, C.Y., Bertoldi, K., Boyce, M.C., Thomas, E.L., 2009. Combining pattern instability and shape-memory hysteresis for phononic switching. Nano Lett. 9, 2113–2119.
Kittel, C., 1986. Introduction to Solid State Physics, seventh ed. Wiley, New York, Chichester.
Kushwaha, M.S., Halevi, P., Dobrzynski, L., Djafari-Rouhani, B., 1993. Acoustic band structure of periodic elastic composites. Phys. Rev. Lett. 71, 2022–2025.
Maldovan, M., Thomas, E.L., 2006. Simultaneous localization of photons and phonons in two-dimensional periodic structures. Appl. Phys. Lett. 88, 251907.
Maldovan, M., Thomas, E.L., 2009. Periodic Materials and Interference Lithography: for Photonics, Phononics and Mechanics. Wiely-VCH Verlag GmbH & Co. KGaA, Weinheim.
Ogden, R.W., 1984. Non-Linear Elastic Deformations. Dover Publications.
Qi, M.H., Lidorikis, E., Rakich, P.T., Johnson, S.G., Joannopoulos, J.D., Ippen, E.P., Smith, H.I., 2004. A three-dimensional optical photonic crystal with designed point defects. Nature 429, 538.
Sainidou, R., Stefanou, N., Modinos, A., 2002. Formation of absolute frequency gaps in three-dimensional solid phononic crystals. Phys. Rev. B 66, 212–301.
Sigalas, M.M., Economou, E.N., 1992. Elastic and acoustic-wave band-structure. J. Sound Vib. 158, 377–382.
Sigalas, M.M., Kushwaha, M.S., Economou, E.N., Kafesaki, M., Psarobas, I.E., Steurer, W., 2005. Classical vibrational modes in phononic lattices: theory and experiment. zeitschrift fur Kristallographie 220, 765–809.
Wang, L.F., Boyce, M.C., Wen, C.Y., Thomas, E.L., 2009. Plastic dissipation mechanisms in periodic microframe-structured polymers. Adv. Func. Mater. 19, 1343–1350.
Yang, S., Megens, M., Aizenberg, J., Wiltzius, P., Chaikin, P.M., Russel, W.B., 2002. Creating periodic three-dimensional structures by multibeam interference of visible laser. Chem. Mater. 14, 2831.